J Nanostruct 15(2): 740-751, Spring 2025

RESEARCH PAPER

Enhancement of the Some Optical Properties of Nanostructure SnS:Cd Films Via by the Spray pyrolysis

Ahmed Nsaif Jasim

Department of Physics, College of Science, University of Diyala, Iraq

ARTICLE INFO

Article History:
Received 18 January 2025
Accepted 21 March 2025
Published 01 April 2025

Keywords:
CSP
Doping
Optical properties
Topography
XRD

ABSTRACT

SnS:Cd nanostructured thin films were produced via chemical spray pyrolysis (CSP). XRD analysis shows an orthorhombic structure. The film with 4% Cd-SnS demonstrated favorable structural attributes, featuring a large crystallite size of 13.44 nm and a small dislocation line density of 5.355 × 10^{15} lines/m^2. SEM images revealed noticeable surface transformations in SnS films, characterized by uniform spherical nano-grains following Cadmium doping. Cadmium doping decreased the bandgap energy (Eg) of SnS, with the lowest value of (1.35 eV) observed at 4% Cd doping in SnS. Undoped SnS had lowest resistance; 4% Cd doping increased resistance via electron extraction. NO_2 exposure decreased resistance via oxygen ion concentration change. The sensitivity decreases with cadmium doping in SnS, impacting NO_2 exposure response. Higher doping reduces responsiveness due to increased charge carrier recombination.

How to cite this article
Jasim A. Enhancement of the Some Optical Properties of Nanostructure SnS:Cd Films Via by the Spray pyrolysis. J Nanostruct, 2025; 15(2):740-751. DOI: 10.22052/JNS.2025.02.032

INTRODUCTION

SnS, part of the IV–VI group, is a p-type semiconductor. It boasts excellent thermal and chemical stability, featuring indirect (1 to 1.5 eV) and direct band gaps (1.39 to 2.33 eV), whose specific values vary based on preparation method and heat treatment temperature. [1-4]. Doping is the most effective method for improving the physical characterization while preserving crystal structure. Different metals, such as Bi, Sb, Ag, Cu, and Cd, have been employed as dopants in SnS [5]. Cadmium has emerged as the most preferable dopant for SnS, thanks to its unique electrical and optical attributes when combined with sulfide [6]. Specifically, Cadmium stands out as a promising candidate for doping SnS thin films because of the favorable ionic radii of the dopant cation Cd^{2+} (114 pm or 0.95 Å), which compares favorably to that of the Sn^{2+} ion (118 pm or 0.93 Å) [7,8]. Since SnS has limited vacant sites, an abundance of Cd accumulates on the surface rather than substituting within the crystal lattice, leading to reduced crystallinity and an increased bandgap. Several methods have been employed for thin film preparation, including DC and RF magnetron sputtering [9,10], pulse electro-deposition [11], thermal evaporation [12], CBD [13], and CSP [14]. Chemical spray pyrolysis (CSP) is relatively simpler, faster, and more cost-effective than these methods.

MATERIALS AND METHODS

Thin films of SnS and SnS:Cd were fabricated using chemical spray pyrolysis (CSB). A custom-designed glass atomizer with a 1 mm output nozzle diameter sprayed a 0.1 M solution of Sn [$C_4H_6CuO_4$] onto glass bases at 400°C. For doping,

* *Corresponding Author Email: ahmedphy@uodiyala.edu.iq*

$CdCl_3$ was dissolved in redistilled water, with drops of HCl added until the solution turned clear. Table 1 outlines the optimal deposition parameters.

Weighing was done on specimens both prior to and after spraying. to ascertain film mass. Film thickness, determined via the weighing method, measured 330 ± 30 nm. Structural properties were evaluated using XRD, while AFM was utilized to analyze the film surface. Scanning electron microscopy (SEM) was utilized for morphological analysis. Additionally, absorption and transmission spectra were analyzed using a double-beam UV/VIS spectrophotometer.Gas sensitivity was evaluated by determining the resistance percentage change in a cylindrical chamber measuring 8 cm in radius and 18 cm in height.

RESULTS AND DISCUSSION

XRD patterns of Cd-doped SnS films with varying Cadmium concentrations (0 wt%, 2 wt%, and 4 wt%) are depicted in Fig. 1. The peaks that represent SnS were at 2θ of 28.56°, 34.32°, 47.77°, and 56.64°, attributed to the (008), (106), (110), and (118) planes respectively, were observed. These findings confirm the crystalline orthorhombic structure of the pure SnS film, which aligns well with the standard JCPDS card No (39-1363). Compared to previously fabricated

Table 1 outlines the optimal deposition parameters for spray solutions.

Specimen	2 (°)	(hkl) Plane	FWHM (°)	Optical bandgap (eV)	Grain size (nm)	Dislocations density ($\times 10^{14}$) (lines/m^2)	Strain ($\times 10^{-4}$)
Undoped SnS	28.56	008	0.69	1.47	11.88	70.80	29.17
SnS: 2% Cd	28.53	008	0.66	1.41	12.42	64.77	27.90
SnS: 4% Cd	28.51	008	0.61	1.35	13.44	55.35	25.79

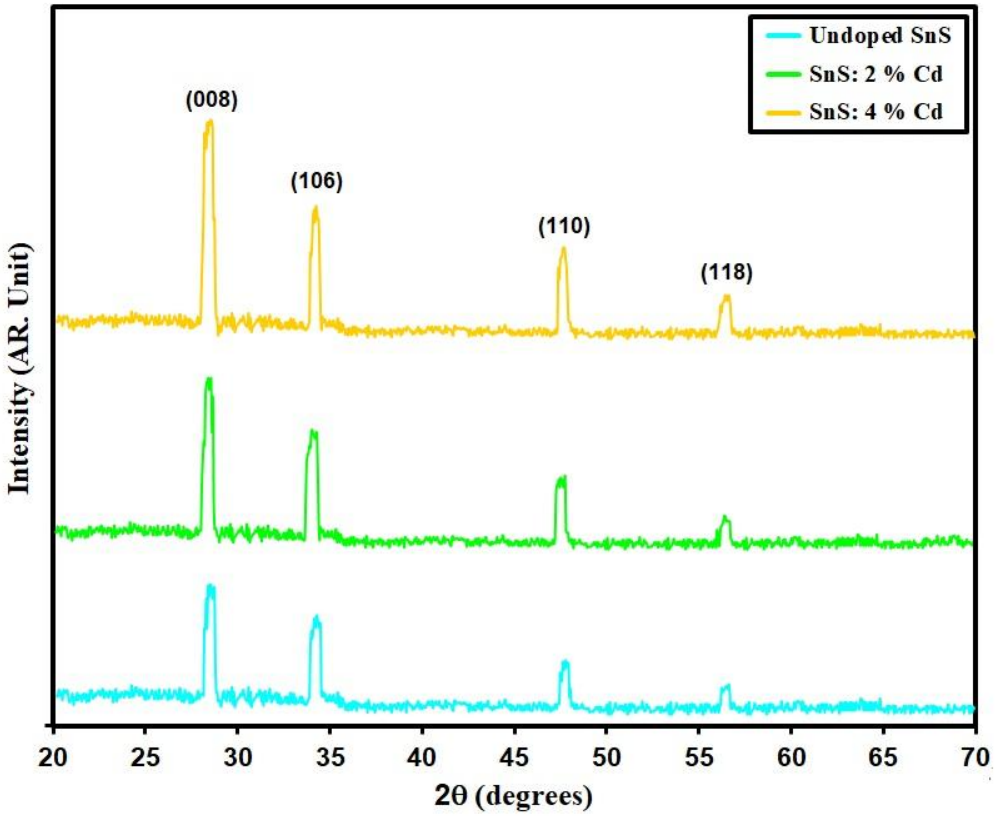

Fig.1. XRD styles of grown films.

films, this film exhibits good crystallinity. When 2% Cd is introduced as a dopant into SnS, there is an increase in peak intensity and a slight shifting at 2θ values of 34.32°. This minor intensity increase and peak shifting confirm the doping process. The observed peak shifting is attributed to differences in atomic size, which lead to expansion or contraction of repetition lengths in the crystal structure depending on the dopant concentration relative to the host atoms. The variation in peak intensities is attributed to doped atoms differing from the host atoms [15]. The increase in intensity suggests an enhancement in layer orientation and crystalline quality [16]. The enhancement in crystalline quality is notably evident with the heightened peak intensity observed at 4% Cadmium doping in SnS. Improved layer orientation and crystal quality correlate with a steady rise in the intensity of the same diffraction peak. The formation of the orthorhombic phase is directly associated with the rock-salt content [17]. However, lattice disorder arises due to significant Cadmium dopants, generating stress. These stresses impede grain growth [18].

The crystallite size (D), is calculated using Scherrer's formula [19]:

$$D = \frac{K\lambda}{\beta\cos\theta} \quad (1)$$

If we denote *K* as (0.9), λ is radiation wavelength, and θ as Bragg's angle, β, is FWHM. According to Scherrer's formula, an increase in crystallite size (D) from 11 nm to 23 nm is observed due to Cd doping at 2% and 4% concentrations. Better crystal development results from this, especially at grain boundaries.The presence of Cd atoms in the correct lattice positions within the SnS film structure is likely responsible for this increase in D. Additionally, because Cd functions as an enhancer instead than an inhibitor, the low value of D seen with cadmium doping suggests a decrease in crystal defects [20]. The dislocation density (δ) was determined via the formula [21].

$$\delta = \frac{1}{D^2} \quad (2)$$

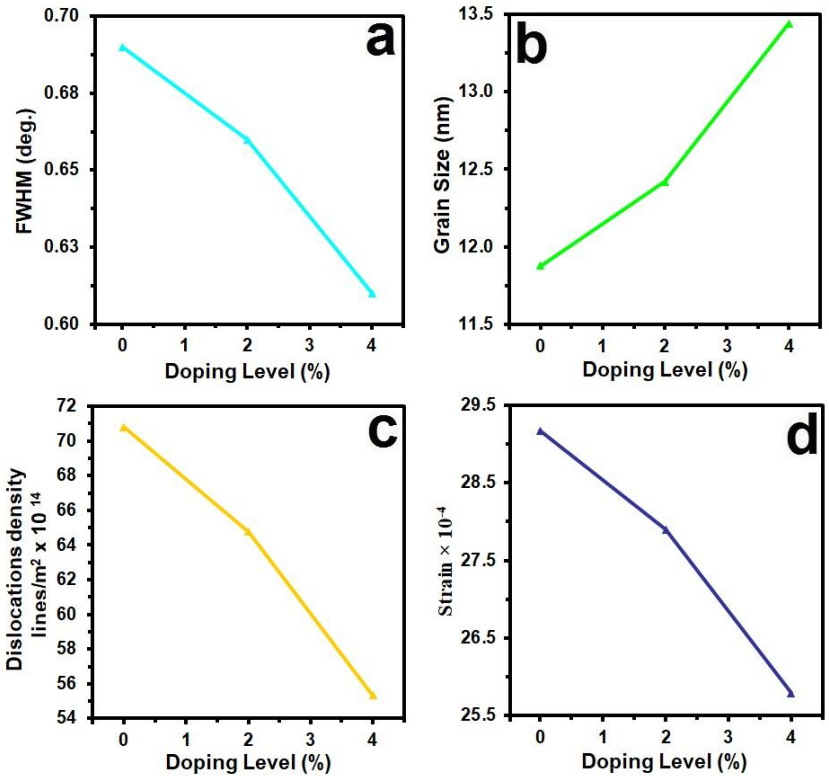

Fig. 2. FWHM, strain and dislocation of pure and SnS:Cd films with different dopants.

Strain (ε) was calculated using the formula [21].

$$\varepsilon = \frac{\beta \cos\theta}{4} \quad (3)$$

Fig. 2 shows that δ and ε initially decrease with increasing doping concentration. The pure SnS films have the lowest values of (δ) and (ε), suggesting less grain boundaries and stronger stability in thin films. Lattice dilatation could cause the observed variation in SnS thin film crystallite size [22]. Table 2 presents D and δ for different doping content.

AFM was employed to examine the surface topography as depicted in the 2D images presented in Fig. 3. The incorporation of Cd into the SnS matrix resulted in changes in the topological properties, as confirmed by the 2D images. Surface roughness dropped from 11.5 nm to 2.63 nm when the doping concentration rose from 0% to 2% and 4%, presumably due to the surface's suppressed cadmium segregation.

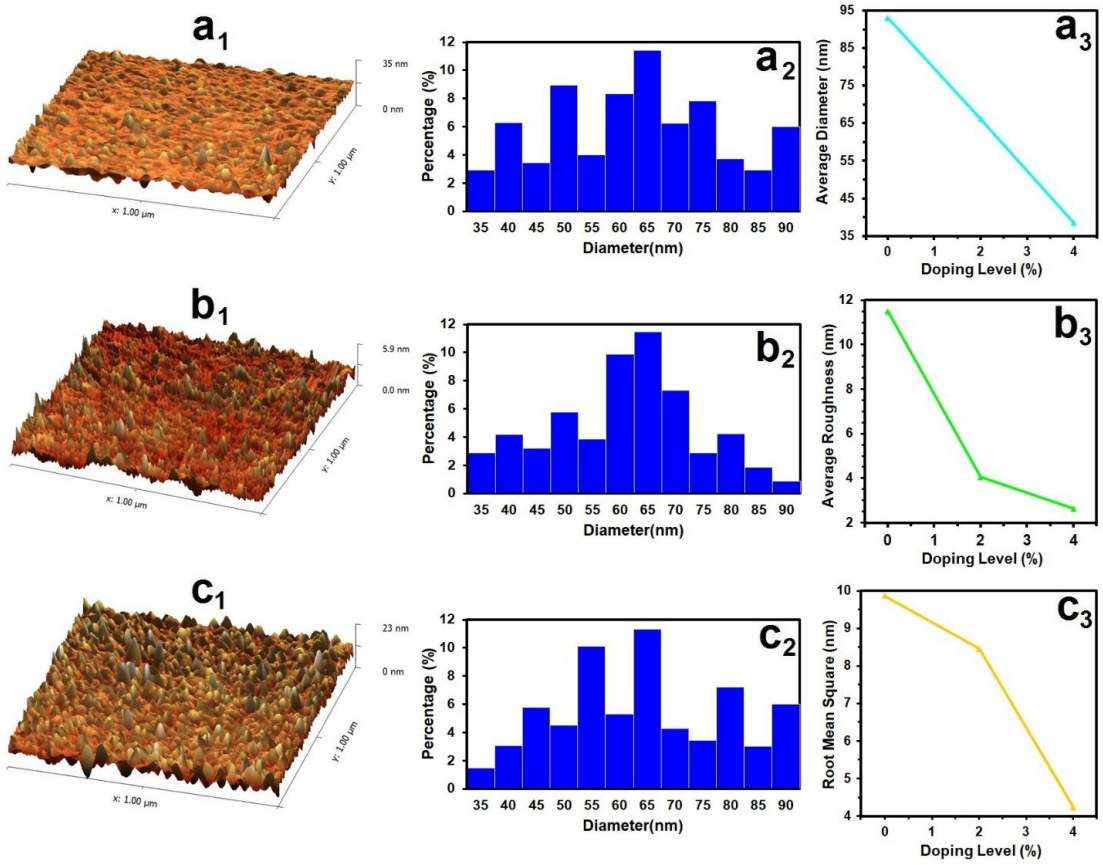

Fig. 3. AFM information.

Table 2. Structural parameters of pure SnS and doping with Cadmium films.

Samples	D (nm)	R_a (nm)	RMS (nm)
SnS	93.1	11.50	9.87
SnS: 2% Cd	66.2	4.05	8.46
SnS: 4% Cd	38.6	2.63	4.23

Figs. 3a, 3b, and 3c illustrate surface textures with hillock-like topology for pure SnS and doping concentrations of 2% and 4%, respectively. Consequently, the film surfaces appeared smoother than those prepared with pure SnS. The difference between the crystallite size calculated using Scherrer's Equation and AFM arises from the fact that a grain comprises several aggregated crystallites. A more significant number of smaller crystallites are formed due to increased doping. This behaviour could be explained by doping producing a larger density of nucleation centres, which leads to a higher density of crystallites with smaller diameters [23].

R_a , RMS and *D* for all samples are summarized in Table 2.

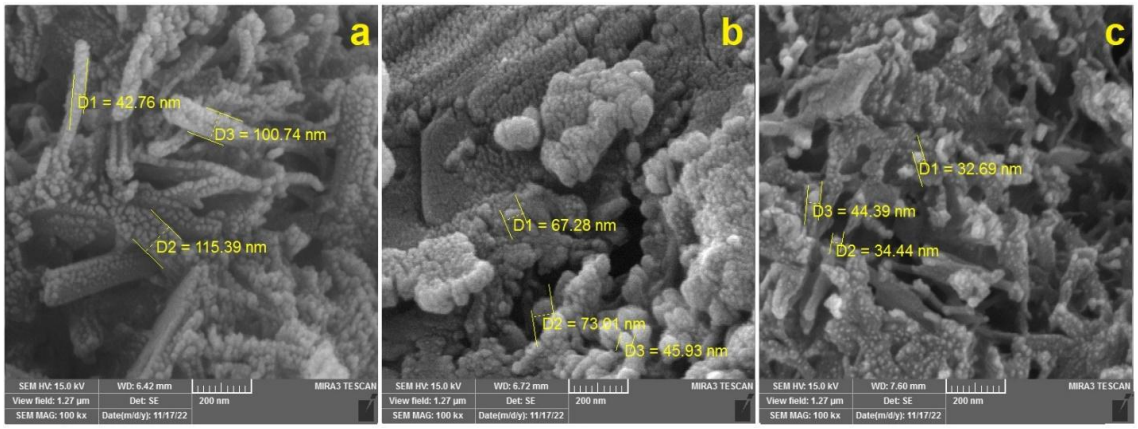

Fig. 4. SEM of grown films.

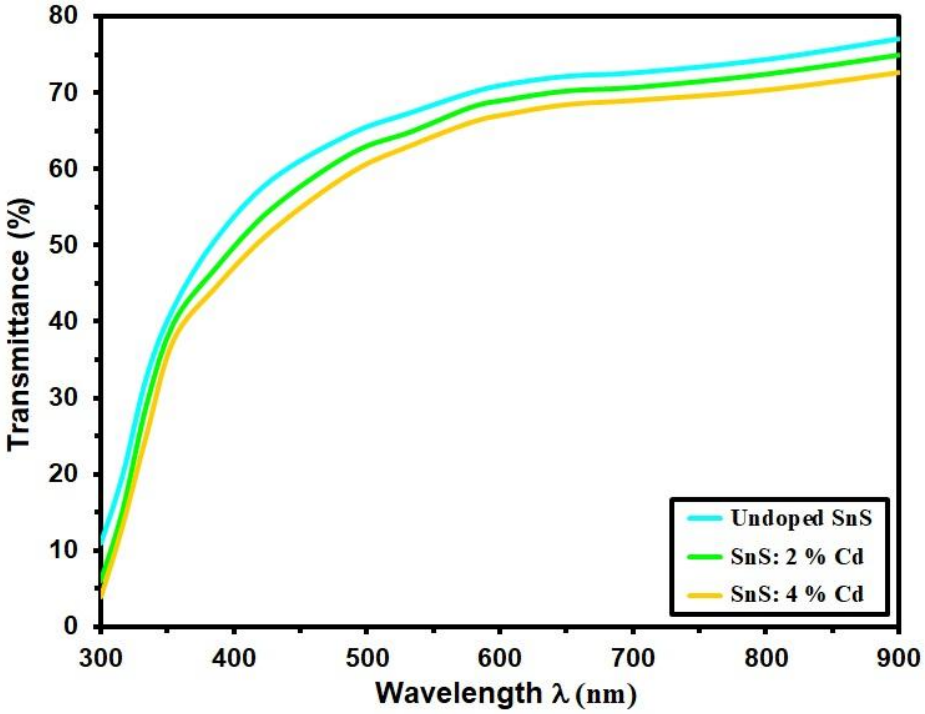

Fig. 5. Transmittance of grown films.

The SEM images presented in Fig. 4 (a), (b), and (c) provide a visual depiction of the surface morphology of SnS, SnS: 2% Cd, and SnS: 4% Cd thin films, respectively. A noticeable trend is observed wherein there is a gradual decrease in grain size with increasing Cadmium doping concentration. Additionally, it's important to note that the surface morphology of films containing SnS: 2% Cd and SnS: 4% Cd exhibits slight deviations compared to that of Undoped SnS. These observed variations in morphology can be attributed to several factors, including variances in the lattice structure induced by Cadmium doping and deposition-induced defects. Incorporating Cadmium atoms into the SnS lattice may lead to structural distortions, affecting the nucleation and growth of grains during film deposition. Additionally, deposition processes can introduce defects in the film structure, further influencing its surface morphology.

Transmittance (T), is defined by Equation [20-21]:

$$T\% = \frac{I}{I_o}\% \quad (4)$$

Here, I_o represents the initial light intensity, and (I) denotes the light intensity after passing through the sample. (T%) of undoped and Cadmium-doped SnS nanocrystalline films deposited at 400°C are presented in Fig. 5. Notably, there's an average T of approximately 75% in the visible region. The absorption spectra of SnS:Cd nanocrystalline thin films are illustrated in Fig. 6. It's observed that the absorption edge (A_e) shifts towards longer λ with increasing doping, indicating a reduction in the energy gap with higher doping levels. The increased number of atoms is the cause of this phenomenon, which offers absorption opportunities for more photons. Similar findings have been reported via reference [24]. The increased absorption with Cadmium doping suggests improved optical properties, potentially beneficial for optoelectronic applications. The shift in A_e towards longer λ indicates a decrease in the bandgap energy, making the material more suitable for absorbing photons with lower energies, thus expanding its spectral response range.

The absorption coefficient (α) corresponding

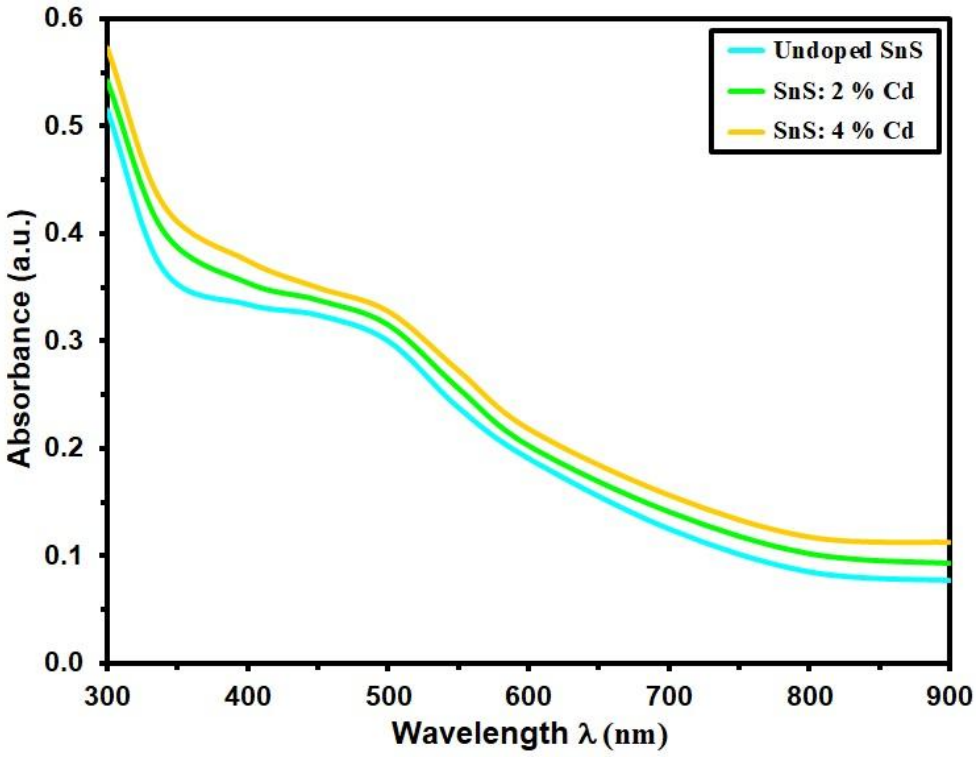

Fig. 6. Absorbance of the entended films.

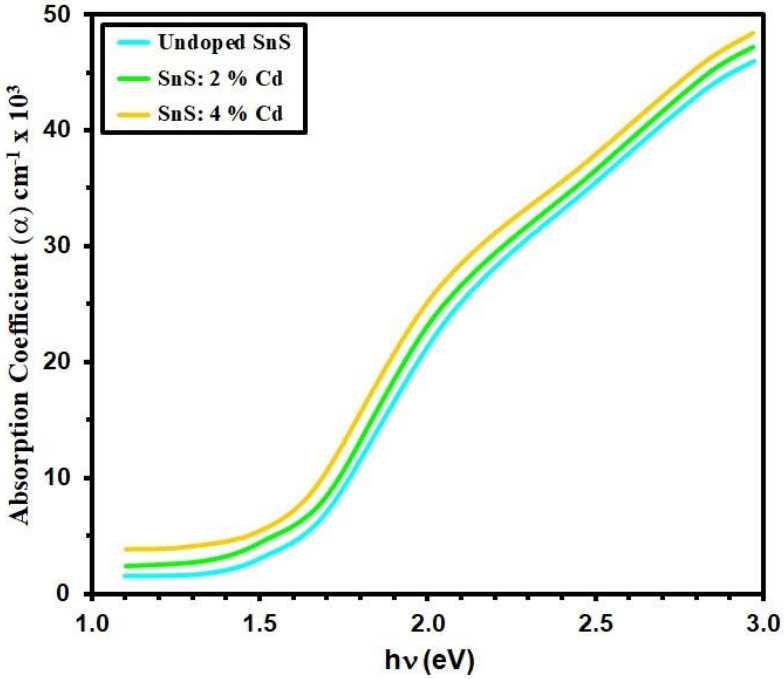

Fig. 7. α of the intended films.

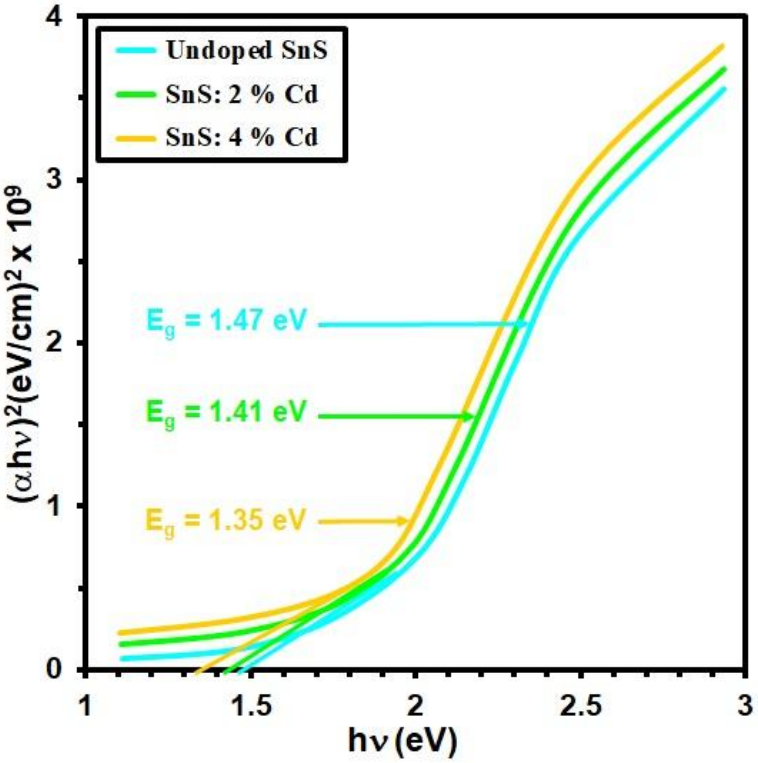

Fig. 8. of the grown films.

to the intense absorption region of the films was determined from the absorbance (A) and the thickness of the film (t) using the following relation [25]:

$$\alpha = \frac{(\ln T^{-1})}{t} \quad (5)$$

The increased absorption coefficient of SnS:Cd nanocrystalline films with doping concentration, as shown in Fig. 7, indicates an enhancement in the material's light absorption capability. This is further supported by the observation that the absorption coefficient (α) exceeds 10^4 cm^{-1}, signifying strong light absorption properties. Additionally, the shift of the A_e towards lower photon energy regions with increasing doping concentration up to 2% suggests a reduction in the optical band gap. This phenomenon may be attributed to the introduction of Cadmium atoms, which can alter the band structure of SnS, leading to a modification in its optical properties. Moreover, unsaturated bonds within the layers could contribute to forming defects in the material. These defects may create localized states in the band structure, effectively reducing the optical band gap. The optical band gap (E_g) can be derived from the optical absorption spectrum using the Tauc relation [27]. This method allows for determining E_g and provides insights into the material's electronic properties and potential applications in optoelectronic devices.

$$\alpha h\upsilon = B(h\upsilon - E_g)^r \quad (6)$$

Where hυ is photon energy, B constant, and r is 0.5 for allowed direct transitions, Fig. 8 displays values of Eg ,which decreased from 1.47 eV for SnS thin films to 1.35 eV for SnS:Cd thin films with a doping content of 4%. This decrease in Eg is significant and is attributable to the influence of cadmium doping. As a result, the material's band structure is modified, causing a reduction in the optical band gap [28].

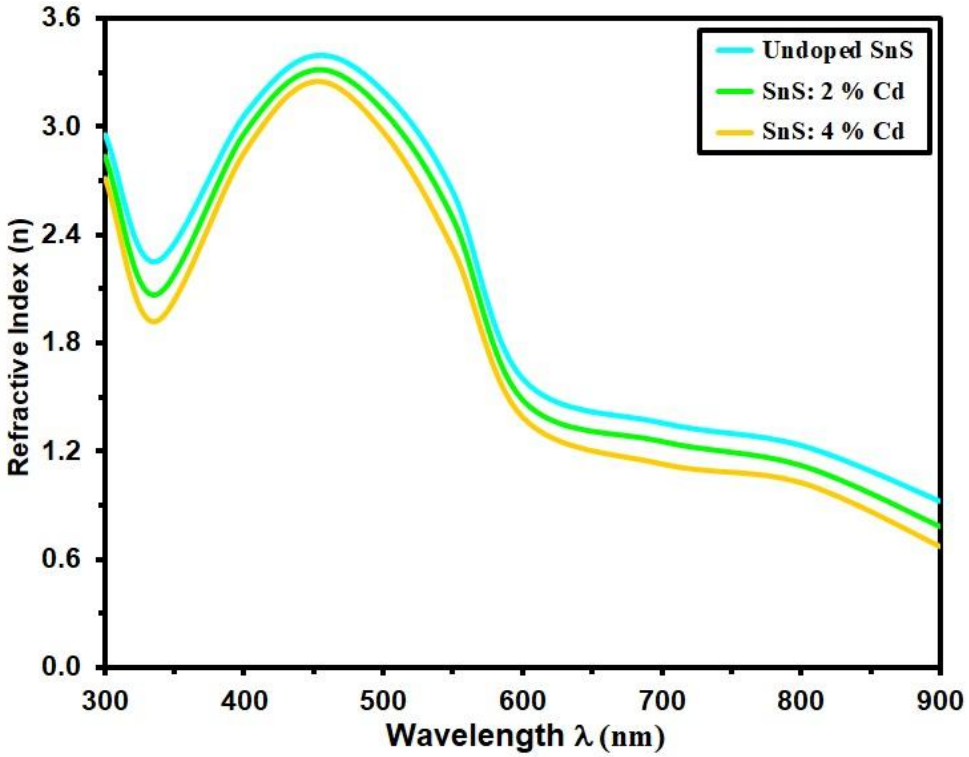

Fig. 9. n of grown films.

The refractive index (n)was determined using the relation [29]:

$$n = \frac{1+R^{\frac{1}{2}}}{1-R^{\frac{1}{2}}} \quad (7)$$

Where R is reflectance. The variation of n with λ is shown in Fig. 9. It was noticed that the refractive index (n) slightly decreased with changes in doping concentration, ranging from 3.40 to 3.24 at a wavelength of 450 nm. This observation suggests that the doping content affects the optical properties of the films. Additionally, the refractive index serves as a qualitative indicator of the surface smoothness and homogeneity of the films [30]. A decrease in refractive index with doping concentration might indicate changes in the material's density or composition, affecting its optical properties.

The extinction coefficient (k) can be determined using the Equation [31]:

$$k = \frac{\alpha\lambda}{4\pi} \quad (8)$$

The behavior of *k* is shown in Fig. 10. From this figure. *k* increases with increasing doping concentration. Specifically, for the as-deposited SnS films, the extinction coefficient (k) increases from 0.51 to 0.55. This behavior can be explained by the increase in absorbance or α, which consequently increases k. Additionally, this increase could be ascribed to the same cause as previously stated regarding n , where the optical energy gap decreases due to the increased absorbance.

Gas sensing properties of Cadmium-doped and undoped SnS nanostructures were investigated for NO_2 at 90°C, with dynamic resistance changes illustrated in Fig. 11. Undoped SnS exhibited the lowest resistance due to its higher roughness, surface area, and porosity, which were observed in AFM and SEM analyses. Electrical resistance data corroborated this finding. All samples exhibited p-type semiconductor behavior. SnS with 4% Cd

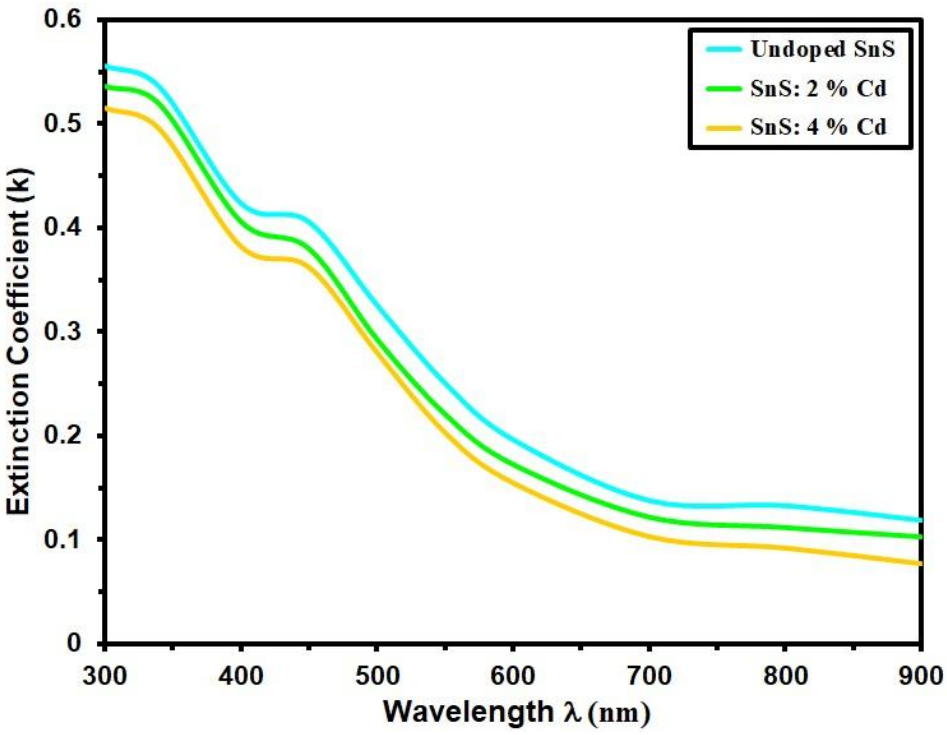

Fig. 10. *k* of the intended.

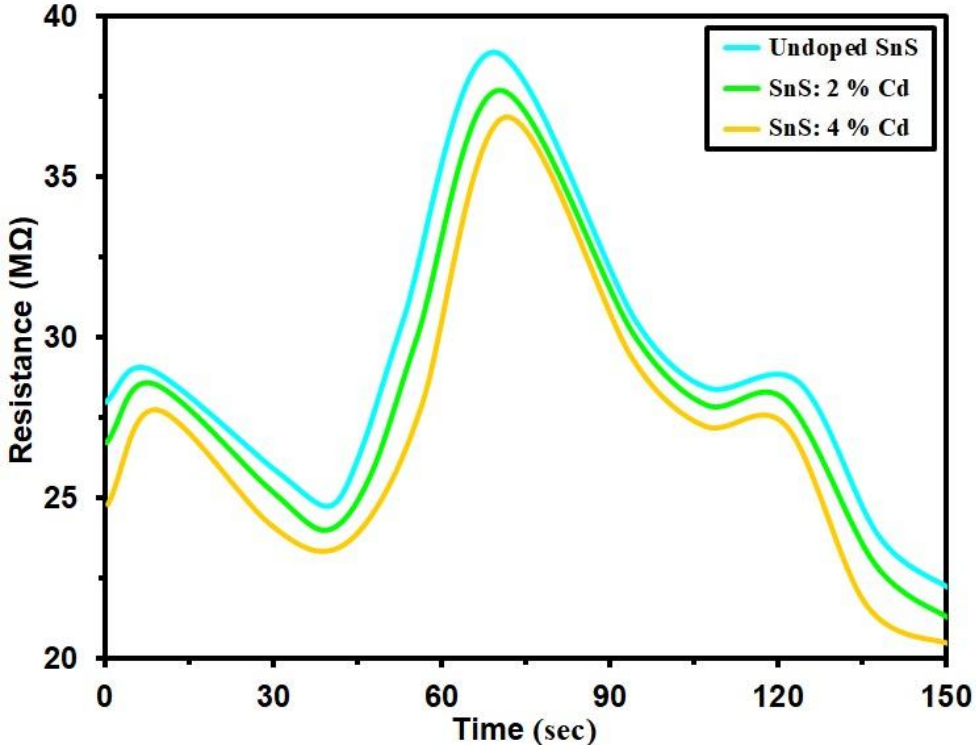

Fig. 11 The resistance versus operating time grown films.

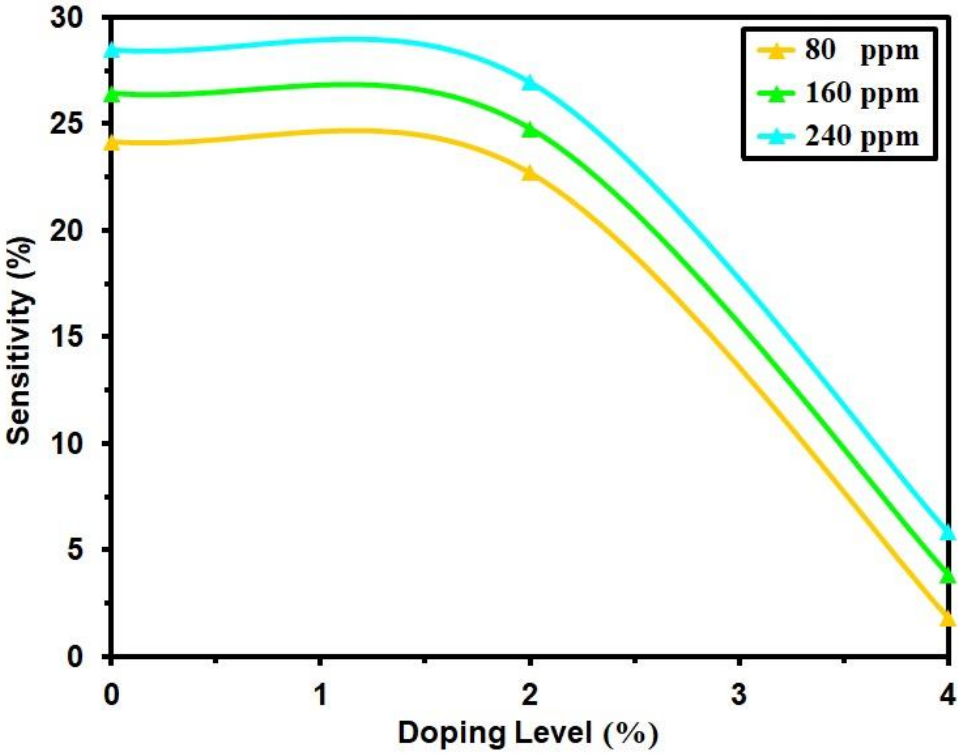

Fig. 12 The sensitivity of undoped SnS and SnS:Cd films with various dopants.

doping displayed the highest resistance, attributed to electron extraction, which increased hole density at the gas-solid interface. This reduced potential barrier for electrons as oxygen ion density on the surface increased, subsequently lowering electrical resistivity. The introduction of NO_2 altered the concentration of oxygen ions, decreasing resistance. This explanation elucidates the observed resistance changes in response to NO_2 exposure.

The sensitivity can be calculated using Eq. 9:

$$\text{Sensitivity} = \frac{\Delta R}{R_g} = \left|\frac{R_g - R_a}{R_g}\right| \times 100\ \% \quad (9)$$

Where Ra R_g is the sensor's resistance in the presence of gas and air. The sensitivity plots in Fig. 12 demonstrate the effect of Undoped, SnS: 2% Cd, and SnS: 4% Cd on NO_2 gas exposure. The recombination process between charge carriers affects sensitivity, showing a decrease with increasing Cadmium doping levels [36]. For Undoped, SnS: 2% Cd, and SnS: 4% Cd, the sensitivity dropped from 24.1 % to 1.8 % (80 ppm), 26.5 % to 3.8 % (160 ppm), and 28.4 % to 5.9 % (240 ppm) [37]. A similar decrease in sensitivity was observed for Undoped, SnS: 2% Cd, and SnS: 4% Cd, indicating that higher Cadmium doping levels result in reduced sensor responsiveness to NO2 gas.This reduction in sensitivity is attributed to the increased recombination rate of charge carriers, which diminishes the number of carriers available to interact with NO_2 gas molecules, lowering the sensor's overall responsiveness.

CONCLUSION

The impact of Cadmium doping on the structural, surface topography, and optical properties of SnS films deposited via CSP technique was investigated. XRD analysis revealed that the films exhibited a polycrystalline nature with a preferred grain orientation along the (008) plane, demonstrating an orthorhombic crystal structure. With the introduction of Cadmium doping, the crystallite size increased from 11.88 nm to 13.44 nm. The film's transmittance in the visible region was above 75%. Furthermore, as the doping concentration increased, E_g value decreased from 1.47 eV to 1.35 eV. AFM images revealed that undoped and Cadmium-doped SnS films consist of rounded-shaped particles. The RMS roughness values decreased with increasing Cadmium dopant concentration, ranging from 9.87 nm to 4.23 nm. SEM images displayed SnS films undergoing a significant surface transformation characterized by uniformly distributed spherical nano-grains following Cadmium doping. Undoped SnS had lowest resistance due to surface properties. 4% Cd doping increased resistance via electron extraction. NO_2 exposure reduced resistance by altering oxygen ion concentration. Higher Cadmium doping decreases sensitivity due to increased charge carrier recombination.

ACKNOWLEDGMENTS

This research is supported by University of Diyala.

CONFLICT OF INTEREST

The authors declare that there is no conflict of interests regarding the publication of this manuscript.

REFERENCES

1. Sousa MG, da Cunha AF, Fernandes PA. Annealing of RF-magnetron sputtered SnS_2 precursors as a new route for single phase SnS thin films. J Alloys Compd. 2014;592:80-85.
2. Liang BYJ, Shen Y-M, Wang S-C, Huang J-L. The influence of reaction temperatures and volume of oleic acid to synthesis SnS nanocrystals by using thermal decomposition method. Thin Solid Films. 2013;549:159-164.
3. Gao W, Cao M, Yang J, Shen J, Huang J, Zhao Y, et al. Controllable synthesis of SnS_2/SnS nanosheets and their photoelectric properties. Mater Lett. 2016;180:284-287.
4. de Kergommeaux A, Faure-Vincent J, Pron A, de Bettignies R, Reiss P. SnS thin films realized from colloidal nanocrystal inks. Thin Solid Films. 2013;535:376-379.
5. Mariappan R, Ponnuswamy V, Suresh P, Suresh R, Ragavendar M, Sankar C. Deposition and characterization of pure and Cd doped SnO_2 thin films by the nebulizer spray pyrolysis (NSP) technique. Mater Sci Semicond Process. 2013;16(3):825-832.
6. Ravichandran K, Saravanakumar K, Chandramohan R, Nandhakumar V. Influence of simultaneous doping of Cd and F on certain physical properties of ZnO nanopowders synthesized via a simple soft chemical route. Appl Surf Sci. 2012;261:405-410.
7. Shahar B, Khan MI, Albalawi H, Islam Gu, Siddique M, Ahmad T, et al. Effect of Cd doping on the structural, optical, and photovoltaic properties of SnS films. Journal of Materials Research and Technology. 2022;19:1982-1992.
8. Bertine KK, Goldberg ED. Fossil Fuel Combustion and the Major Sedimentary Cycle. Science. 1971;173(3993):233-235.
9. Li X-Y, Li H-J, Wang Z-J, Xia H, Xiong Z-Y, Wang J-X, et al. Effect of substrate temperature on the structural and optical

properties of ZnO and Al-doped ZnO thin films prepared by dc magnetron sputtering. Opt Commun. 2009;282(2):247-252.
10. Elanchezhiyan J, Bhuvana KP, Gopalakrishnan N, Shin BC, Lee WJ, Balasubramanian T. Investigations of the properties of $Zn_{1-x}Cr_xO$ thin films grown by RF magnetron sputtering. J Alloys Compd. 2009;478(1-2):45-48.
11. Cheng S, Chen Y, He Y, Chen G. The structure and properties of SnS thin films prepared by pulse electro-deposition. Mater Lett. 2007;61(6):1408-1412.
12. Shah NM, Panchal CJ, Kheraj VA, Ray JR, Desai MS. Growth, structural and optical properties of copper indium diselenide thin films deposited by thermal evaporation method. Solar Energy. 2009;83(5):753-760.
13. Mnari M, Kamoun N, Bonnet J, Dachraoui M. Chemical Bath Deposition of tin sulphide thin films in acid solution. Comptes Rendus Chimie. 2009;12(6-7):824-827.
14. Reddy NK, Reddy KTR. SnS films for photovoltaic applications: Physical investigations on sprayed Sn_xS_y films. Physica B: Condensed Matter. 2005;368(1-4):25-31.
15. Rahdar A, Aliahmad M, Samani M, HeidariMajd M, Susan MABH. Synthesis and characterization of highly efficacious Fe-doped ceria nanoparticles for cytotoxic and antifungal activity. Ceram Int. 2019;45(6):7950-7955.
16. Mehmood B, Khan MI, Iqbal M, Mahmood A, Al-Masry W. Structural and optical properties of Ti and Cu co-doped ZnO thin films for photovoltaic applications of dye sensitized solar cells. International Journal of Energy Research. 2020;45(2):2445-2459.
17. Arulanantham AMS, Valanarasu S, Jeyadheepan K, Kathalingam A. Effect of carrier gas pressure on structural, optical and photovoltaic properties of tin sulphide thin films prepared by nebulizer spray pyrolysis method. Bull Mater Sci. 2019;42(3).
18. Rajesh Kumar B, Hymavathi B. X-ray peak profile analysis of solid-state sintered alumina doped zinc oxide ceramics by Williamson–Hall and size-strain plot methods. Journal of Asian Ceramic Societies. 2017;5(2):94-103.
19. Thaweesaeng N, Suphankij S, Pecharapa W, Techitdheera W. Structural and optical properties of Cu-doped ZnO nanoparticles synthesized by co-precipitation method for solar energy harvesting application. 2013 IEEE 5th International Nanoelectronics Conference (INEC); 2013/01: IEEE; 2013. p. 274-276.
20. Guneri E, Ulutas C, Kirmizigul F, Altindemir G, Gode F, Gumus C. Effect of deposition time on structural, electrical, and optical properties of SnS thin films deposited by chemical bath deposition. Appl Surf Sci. 2010;257(4):1189-1195.
21. Hameed SA, Bakr NA, Hassan AM, Jasim AN. Structural and optical properties of Cu2ZnSnS4 thin films fabricated by chemical spray pyrolysis. AIP Conference Proceedings: AIP Publishing; 2020. p. 020082.
22. Bedir M, Tunç A, Öztas M. Investigation of the Characteristics of the Boron Doped MnO Films Deposited by Spray Pyrolysis Method. Acta Phys Pol, A. 2016;129(6):1159-1164.
23. Sebastian S, Kulandaisamy I, Valanarasu S, Shkir M, Ganesh V, Yahia IS, et al. Physical and electrical properties' evaluation of SnS:Cu thin films. Surf Eng. 2020;37(2):137-147.
24. Kungumadevi L, Sathyamoorthy R, Subbarayan A. AC conductivity and dielectric properties of thermally evaporated PbTe thin films. Solid·State Electron. 2010;54(1):58-62.
25. Hameed SA. Effect of Thickness on Structural and Optical Properties of CdO Thin Films Prepared by Chemical Spray Pyrolysis Method. Neuroquantology. 2020;18(4):20-26.
26. Devika M, Reddy NK, Ramesh K, Gunasekhar KR, Gopal ESR, Reddy KTR. Low Resistive Micrometer-Thick SnS:Ag Films for Optoelectronic Applications. J Electrochem Soc. 2006;153(8):G727.
27. Moss TS, Peacock AG. Infrared optical properties of lead halides. Infrared Phys. 1961;1(1):104.
28. Minami T, Kakumu T, Takeda Y, Takata S. Highly transparent and conductive ZnO/In_2O_3 thin films prepared by d.c. magnetron sputtering. Thin Solid Films. 1996;290-291:1-5.
29. Jasim AN. Temperature of base Effect on Optical Properties of Aluminum Oxide (AL_2O_3) Thin Films Prepared by Chemi-thermal Hydrolysis. Neuroquantology. 2020;18(1):64-69.
30. Subramanian B, Sanjeeviraja C, Jayachandran M. Cathodic electrodeposition and analysis of SnS films for photoelectrochemical cells. Materials Chemistry and Physics. 2001;71(1):40-46.
31. Abed ZA, Al Dulaimi AH, Shatti WA, Jasim AN, Khodair ZT, Khaleel SY. Structural and optical characterization of nanostructured undoped CuO and cobalt - doped CuO thin films. Journal of Ovonic Research. 2021;17(6):581-587.
32. Pankove JI, Kiewit DA. Optical Processes in Semiconductors. J Electrochem Soc. 1972;119(5):156C.
33. Scherr B. America in Contemporary Soviet Literature. By Alayne P. Reilly. New York: New York University Press. London: University of London Press, 1971. xiii, 217 pp. $8.95. Slavic Review. 1972;31(1):199-200.
34. Willeke G, Dasbach R, Sailer B, Bucher E. Thin pyrite (FeS_2) films prepared by magnetron sputtering. Thin Solid Films. 1992;213(2):271-276.
35. Amroun MN, Khadraoui M, Miloua R, Kebbab Z, Sahraoui K. Investigation on the structural, optical and electrical properties of mixed SnS_2—CdS thin films. Optik. 2017;131:152-164.
36. Di Giulio M, Micocci G, Rella R, Siciliano P, Tepore A. Optical absorption and photoconductovity in amorphous indium selenide thin films. Thin Solid Films. 1987;148(3):273-278.
37. Song S, Wei J, He X, Yan G, Jiao M, Zeng W, et al. Oxygen vacancies generated by Sn-doped ZrO_2 promoting the synthesis of dimethyl carbonate from methanol and CO_2. RSC Advances. 2021;11(56):35361-35374.